The Rotation of the White Light Solar Corona at Height 4 R sun from 1996 to 2010: A Tomographical Study of Large Angle and Spectrometric Coronagraph C2 Observations

Morgan, Huw

Published in:
Astrophysical Journal

DOI:
10.1088/0004-637X/738/2/189

Publication date:
2011

Citation for published version (APA):
Morgan, H. (2011). The Rotation of the White Light Solar Corona at Height 4 R sun from 1996 to 2010: A Tomographical Study of Large Angle and Spectrometric Coronagraph C2 Observations. *Astrophysical Journal*, *738*(2), 189. https://doi.org/10.1088/0004-637X/738/2/189

The Astrophysical Journal, 738:189 (14pp), 2011 September 10 doi:10.1088/0004-637X/738/2/189

THE ROTATION OF THE WHITE LIGHT SOLAR CORONA AT HEIGHT 4 $R_\odot$ FROM 1996 TO 2010: A TOMOGRAPHICAL STUDY OF LARGE ANGLE AND SPECTROMETRIC CORONAGRAPH C2 OBSERVATIONS

Huw Morgan
Institute for Astronomy, University of Hawaii, 2680 Woodlawn Drive, Honolulu, HI 96822, USA; hmorgan@ifa.hawaii.edu
Received 2011 May 16; accepted 2011 July 5; published 2011 August 25

ABSTRACT

Solar rotational tomography is applied to Large Angle and Spectrometric Coronagraph (LASCO) C2/*Solar and Heliospheric Observatory* (*SOHO*) observations covering the period 1996–2010, resulting in a set of electron density maps at a height of 4 $R_\odot$ from which rotation rates can be calculated. Large variation of rotation rates is measured. Rates are dominated by the Carrington rotation rate (14.18 deg d^{-1} sidereal), but at times over the solar cycle, rates are measured between −3 and 3 deg d^{-1} relative to the Carrington rotation rate. Rotation rates can vary considerably between latitudes, even between neighboring latitudes. They can remain relatively stable or change smoothly over long periods of times, or can change rather abruptly. There are periods for certain latitudes (for example, the equator at solar maximum) when the movement is dominated by rapid structural reconfiguration, not a coherent rotation. These results raise new questions regarding the link between the Sun and the corona, and provide fresh challenges to interpretations of the coronal structural evolution and the development of large-scale coronal models. In particular, can interchange reconnection provide an explanation of the considerable latitudinal differences in rotation rates, and what mechanism can explain abrupt changes in rotation rates?

Key words: solar wind – Sun: corona – Sun: rotation

1. INTRODUCTION

Due initially to the dedication of astronomers such as Carrington in the 19th century, the rotation of the Sun has been an active field of research for a century and a half. It is a complicated subject because of the rich variation of results arising from a broad range of observations and analysis techniques. The variation of results is a symptom of the complexity of the Sun's rotation arising from the interdependence of the solar magnetic dynamo with the convective plasma, a relation which gives a rotation which is dependent on latitude and depth within the Sun. It also shows time variation through a dependence on the solar cycle. This variation is fascinating when one considers the huge energies required to cause even a small change in angular momentum. Reviews of the field are given by Howard (1984), Schroeter (1985), and Beck (2000). A detailed review of solar rotation in the context of helioseismology and its relevance to stellar rotation is given by Thompson et al. (2003).

The rotation of the corona is a subject closely linked to that of the Sun's rotation. It has been measured using several different types of observations. For heights above the very lowest corona, most of these are off-limb remote observations of the optically thin plasma; therefore they are line-of-sight (LOS) integrations of electron or ion emission. Consistent sets of observations made over long timescales can then allow a time analysis. As coronal structures of various brightness rotate in and out of the field of view, the flux modulation gives an estimate of the main rotation rate. This is in contrast to typical techniques used for the photosphere, chromosphere, and features in the lowest corona, where spectroscopy can reveal a Doppler shift, or features can be tracked across the disk and from one rotation to the next ("tracer" measurements). The coronal rotation, therefore, has not been measured with the high time resolution and accuracy of photospheric, chromospheric, and low-coronal measurements. Flux modulation must use long time series to more accurately determine the rotation rate (typically several months to a year), but this hides information regarding changes in rotation rate which occur on shorter timescales. Section 7 of Schroeter (1985) states that "we are still far away from having a clear picture of the differential rotation of chromospheric and coronal layers." One of the main reasons for this is the LOS problem associated with remote coronal observations. We lack the ability to make the detailed spectroscopic and tracer measurements which have been made for the photosphere and chromosphere.

This article is concerned with coronal rotation at a height of 4 $R_\odot$. This is a height where the coronal structure is predominately radial, and there is no further large-scale reconfiguration of the magnetic field structure with height. For this reason, the important body of work studying rotation using observations of the chromosphere and very lowest corona are not detailed here, although ultimately they must bear relevance in linking our results with the general solar rotation. These studies include impressive measurements of coronal bright points using extreme-ultraviolet (EUV) images (Wöhl et al. 2010; Zaatri et al. 2009; Karachik et al. 2006, and references within), X-ray bright points (Hara 2009; Kariyappa 2008, and references within), microwave and radio observations of the corona (Vats & Chandra 2011; Mouradian et al. 2002; Brajša et al. 2000, and references within), and observations of filaments, calcium plage, and faculae (Gigolashvili et al. 2007; Brajsa et al. 1991; Ternullo 1987; Adams & Tang 1977, and references within).

Ground-based observations of the corona offer a long time-base of coherent measurements which is useful for time analysis. Flux modulation studies of emission lines (most notably the 5303 Å Fe XIV green line; Jordan 1969; Sime et al. 1989) are generally limited to heights of 0.01–0.25 $R_\odot$ above the limb (Antonucci & Svalgaard 1974; Antonucci & Dodero 1977; Sykora 1994; Makarov & Tlatov 1997; Altrock 2003; Badalyan et al. 2006; Tlatov 2006; Badalyan 2010). Ground-based white light coronagraph observations offer relatively clean signal to heliocentric heights of 2 $R_\odot$ or more, extending the useful height range of flux modulation studies (Hansen et al. 1969; Parker

et al. 1982; Fisher & Sime 1984). Hoeksema & Scherrer (1987) applied a time analysis to the results of a potential field source surface (PFSS) model, which is an extrapolated estimate of the coronal magnetic field based on the observed photospheric field. Direct observations of coronal holes in the lowest corona offer a tracer-type measurement of the coronal rotation in extreme-ultraviolet (EUV), soft X-ray, or near-infrared (NIR) observations (Timothy et al. 1975; Shelke & Pande 1985; Navarro-Peralta & Sanchez-Ibarra 1994; Obridko & Shelting 1989; Insley et al. 1995).

Space-based observations offer continuous sets of coherent observations which are well suited for flux modulation studies. Studies using soft X-ray observations have been made by Weber et al. (1999) and Chandra et al. (2010). In the *Solar and Heliospheric Observatory* (*SOHO*) era, high time resolution and continuous sets of coherent observations over several years have enabled several detailed studies of the coronal rotation at increased height ranges. Flux modulation studies of ultraviolet observations at solar minimum (Giordano & Mancuso 2008) and solar maximum (Mancuso & Giordano 2011) have been made using data from the Ultraviolet Coronagraph Spectrometer (UVCS) instrument aboard *SOHO*, and of white light coronagraph observations at solar minimum (Lewis et al. 1999) and maximum (Lewis & Simnett 2001) using data from the Large Angle and Spectrometric Coronagraph (LASCO; Brueckner et al. 1995) instrument aboard *SOHO*. Since these studies are made at extended heights in the corona, similar to that of this study, they are discussed in more detail below.

The main findings of the ground- and space-based observational studies are summarized here. Particular emphasis has been given to the *SOHO*-based findings, which are made at heights close to those of this study.

1. Close to the equator, the corona rotates at approximately the same rate as sunspots (Hansen et al. 1969; Fisher & Sime 1984; Weber et al. 1999, for example). Using flux modulation of LASCO data, Lewis et al. (1999) found sidereal rotation rates of 14 deg d^{-1} at solar minimum—a rate which was, within uncertainty, constant over heights between 2.5 and 15 $R_\odot$.
2. The corona rotates more rigidly than the photosphere (less differential rotation). Toward mid-latitudes and above, a marked difference in rotation rates is found between the corona and photosphere, with the corona rotating faster than the photosphere (Hansen et al. 1969; Fisher & Sime 1984; Weber et al. 1999; Parker et al. 1982; Chandra et al. 2010; Timothy et al. 1975; Insley et al. 1995; Hoeksema & Scherrer 1987, for example). The latitude where the difference in rotation rates becomes significant and the amount of rigidity differs from study to study. Lewis et al. (1999) measure a latitudinal rigidity in the rotation between $\pm 45^\circ$ of the equator, but suggested that this was due to the influence of equatorial structures projecting along the LOS. They also state that the solar minimum flux modulation was dominated by an active region; therefore the rotation rates would be dominated by that structure. At a height of 1.5 $R_\odot$, Giordano & Mancuso (2008) found equatorial rotation of 14.11 deg d^{-1}, decreasing to 13.8 deg d^{-1} at latitude -30° (south), and 14.07 deg d^{-1} at 30° (north). The solar maximum study of Lewis & Simnett (2001) should, in principle, reveal more accurately the degree of latitudinal rigidity since high-density structures are more evenly distributed in latitude. The rotation at solar maximum was not significantly faster than at minimum, and the rotation was rigid compared to the photosphere. Similar findings were given by the solar maximum study of Mancuso & Giordano (2011). Giordano & Mancuso (2008) interpret abrupt differences in rotation rates at mid-latitudes as boundaries between open and closed field line regions.
3. There is a relationship between solar cycle and the degree of rotational rigidity (Antonucci & Dodero 1977; Sime et al. 1989; Badalyan et al. 2006; Chandra et al. 2010). In times of activity decline the corona rotates more rigidly, and differential rotation is most pronounced in the period of rising and maximum activity. Parker et al. (1982) measured a rotational acceleration of 6% between 1966 and 1976, and suggested a link between coronal structure and layers at depth in the Sun. There are rotational variation patterns over timescales longer than an activity cycle (Tlatov 2006), and there is latitudinal migration of zones of slow rotation rates (Makarov & Tlatov 1997).
4. Many of these studies have found a north–south asymmetry in rotation rates (Hansen et al. 1969; Hoeksema & Scherrer 1987; Giordano & Mancuso 2008).
5. Badalyan et al. (2006) and others previously (for example, Sykora 1994) suggest that the rotation can be interpreted as the superposition of two coexisting modes of rotation—fast and slow, with faster or slower rotation being detected as the relative strengths of the two modes change. Hoeksema & Scherrer (1987) showed that there seemed to be two rotational periods in coexistence of 27 and 28 days (synodic).
6. There may be a height dependence of rotation rates. Hansen et al. (1969) found a height dependence between their observations at 1.125 and 2.0 $R_\odot$ during 1966 but not for 1967. Parker et al. (1982) used the same data set extended to 1976 (i.e., throughout solar cycle 20), and found more rigid rotation at 1.5 $R_\odot$ compared to 1.125 $R_\odot$. Studies of height dependence became more feasible in the *SOHO* era. Lewis et al. (1999) found that the green line corona below 2 $R_\odot$ rotated at 14.15 deg d^{-1}, compared with 14 deg d^{-1} above 2.5 $R_\odot$. Giordano & Mancuso (2008) found a significant decrease of a few percent in the rotation rate between 1.5 and 2.3 $R_\odot$, with the most abrupt change between 2.3 and 2.5 $R_\odot$.
7. There is a link between the lifetime of structures and their rotational rate. Antonucci & Svalgaard (1974) found that short-lived structures rotated more differentially than long-lived structures. As stated by Hoeksema & Scherrer (1987), it is possible that at the photosphere the larger-scale and longer-lived fields are rotating more rigidly than the small-scale fields—and it is these larger-scale fields which most strongly influence the large-scale coronal structure. Fisher & Sime (1984) showed that the estimated lifetime of structure was dependent on solar cycle. Lewis et al. (1999) showed using a simple correlation argument that structures were short-lived during solar maximum compared to minimum, making flux modulation measurements more difficult.

Efforts are being made to reconcile the detected coronal rotational patterns with rotations detected in the convective zone using helioseismology (see Badalyan 2010, and references within). A model framework to explain the coexistence of a rigidly rotating coronal hole with differentially rotating active regions was established by Nash et al. (1988). In the current-free model, the open field lines at the boundary of the coronal holes reconnected ("interchange reconnection") with the neighboring closed field lines. Appropriate rates of interchange reconnection

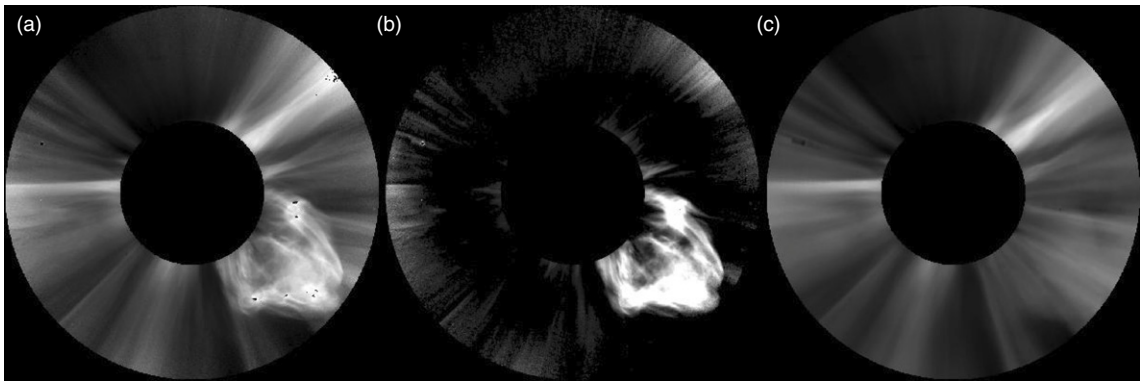

Figure 1. Example of the CME separation process. (a) Normalizing Radial Graded Filter (NRGF) image of a LASCO C2 total brightness observation made at 2002 August 22 02:06. See Morgan et al. (2006) for details of the NRGF process. A large CME is clearly seen in the southwest. (b) The CME signal (and other small events and noise) isolated from the NRGF image using an iterative deconvolution technique based on the ideas presented in Morgan & Habbal (2010a). (c) The corona with the CME signal and noise greatly reduced. This cleaned image is suitable for tomography.

allow different rates of rotation for coronal holes and active regions (Wang & Sheeley 2004; Fisk 2001; Lionello et al. 2005). Current sophisticated models of the global solar corona include differential rotation since many aspects of the corona's structural time evolution are driven by it (see, for example, Mackay et al. 2002), and it can even possibly drive the onset of some coronal mass ejections (CMEs; Wolfson et al. 1996).

The broad range of results and differences between these studies reflect the difficulty of calculating the rotational rate of the extended solar corona from a temporal study of coronagraph images or similar data, since the three-dimensional (3D) structure is not resolved, resulting in an ambiguity relating to the exact distribution of structures along the LOS. Solar rotational tomography (SRT) is a method to reduce this uncertainty. SRT aims to find the 3D distribution of electron density which best satisfies a set of coronagraphic white light observations made over a period of time (typically half a solar rotation for a full reconstruction using one coronagraph). Frazin (2000) gives a good summary of the field. Morgan et al. (2009) introduced a new SRT approach based on Fourier backprojection of height-normalized coronagraph images (Morgan et al. 2006). A comprehensive overview of the changing coronal structure revealed by tomography over a solar activity cycle is given by Morgan & Habbal (2010b), with selected case studies of certain Carrington rotations. This work uses a large set of tomography maps to determine the rotation of the corona—it is therefore a fundamentally different approach to flux modulation, and is more similar to tracer methods. This paper is accompanied by a complementary study (Morgan 2011) which shows how density structures can drift longitudinally along the heliospheric current sheet during solar minimum.

The structure of this work is as follows: Section 2 summarizes the data processing, tomography, and rotational analysis methods. The results of the rotational analysis are given in Section 3 for different phases of the activity cycle. The results are discussed in Section 4. Conclusions are given in Section 5.

2. METHOD

Rotation rate units are given in sidereal degree per day, deg d^{-1}, and are often given relative to the sidereal Carrington rotation rate of 14.18 deg d^{-1} (or a sidereal rotation period of 25.38 days). Conversions from synodic to sidereal are made using the formulation of Roša et al. (1995).

The method is presented in two sections. Section 2.1 briefly describes the data preprocessing steps and tomography, the details of which have been described elsewhere. Section 2.2 shows how a correlation analysis can reveal trends in coronal rotation over the course of a few months.

2.1. Preprocessing and Tomography

The most common observation mode for the LASCO C2 coronagraph (Brueckner et al. 1995) is to make a total brightness observation approximately every 20 minutes. Observations made over half a solar rotation are needed to create one tomography map, and, assuming uninterrupted observations, this is a data set containing typically a thousand images. CMEs are rapid events which disrupt the tomographical process, and a CME separation technique based on ideas described by Morgan & Habbal (2010a) is used to lessen their influence. For example, Figure 1(a) shows an image with a large CME which would usually cause large errors in the tomographical process. The CME removal process isolates and subtracts the CME shown in Figure 1(b) to give an image which gives less error in the tomography process, shown in Figure 1(c).

A thousand images is not necessary for the tomography, and is too large a number for our computational resources; therefore the number is curtailed by around a third to one observation an hour. Further data processing steps, and the main Fourier backprojection tomographical technique, are described in full by Morgan et al. (2009). The tomography reconstructions made for this work are shells of the corona at a height of 4 $R_{\odot}$, with 720 longitude bins and 360 latitude bins. An example of such a map is shown in Figure 2. The maps do not show the electron density directly—rather they show a normalized density, as explained in Morgan et al. (2009). However, they do contain information on the spatial distribution of streamers throughout the corona, as demonstrated by Morgan & Habbal (2010b). The time period of half a solar rotation necessary to create one tomography map can be incremented in time, creating a sliding window throughout the whole LASCO data set from 1996 February to 2010 March. The time increment used is approximately 7 hr. Despite numerous data gaps and unsuccessful tomographical reconstructions, the final number of maps produced is almost 1.3×10^3.

2.2. Long-term Correlation Analysis

Longitudinal density profiles along constant latitudes are extracted from the density maps. For example, it is easy to take a horizontal slice along a constant latitude within a density map

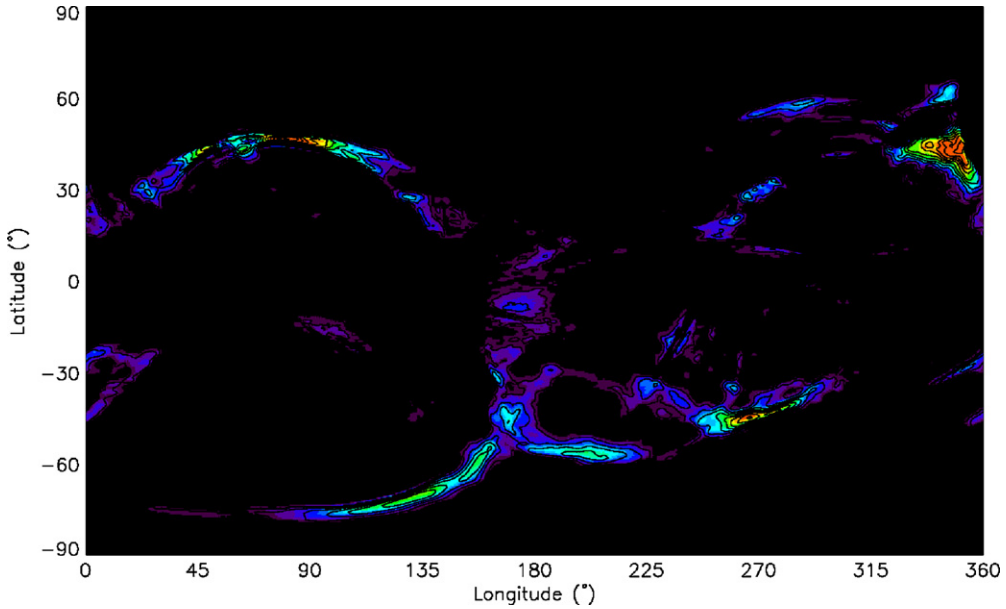

Figure 2. Longitude–latitude map of the coronal density distribution at a height of 4 $R_{\odot}$ determined using the tomography technique for LASCO C2 data observed during the period 2003 January 22 to 2003 February 05. Red is highest density, black regions are those masked to zero since they do not contain any significant high-density structures (see the text).

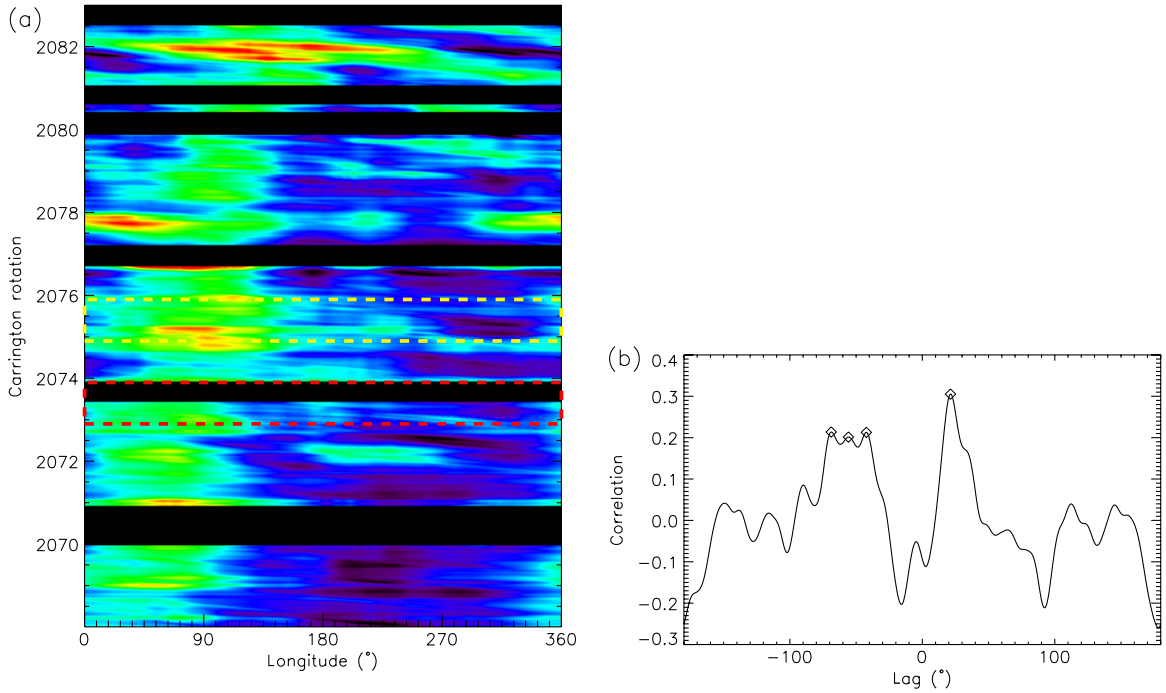

Figure 3. (a) Density at latitude 0° (equator) and height 4 $R_{\odot}$ as a function of longitude and time (or Carrington rotation). Similar to the longitude–latitude map of Figure 2, high-density regions are red, and low density are black/purple. Data gaps are horizontal black strips. Longitudinal drifts of streamers with time are obvious as the slanted structure. The red box encompasses a span of time of two Carrington rotations starting at CR 2072.9. The yellow box is the same length of time but starting 2CR later, at CR 2074.9. (b) The total cross-correlation profile of the two regions boxed in red and yellow in part (a), as described in the text. The diamonds are peaks above a correlation of 0.1, which may be used for higher-level analysis according to several criteria (see the text).

(such as that shown in Figure 2) to give a longitudinal profile of density at that latitude. An extended time series of such longitudinal profiles is very suitable for a correlation analysis. An example of such density profiles, stacked against time, is shown in the contour plot of Figure 3(a). For the sake of example, only a time range between CR 2068 and 2083 is shown here, at a latitude of 0°. Even to the eye, there is a clear longitudinal drift of structure in this longitude–time map. The main high-density structure leans to the right and therefore drifts to increasing longitude with time. This streamer is approximately centered at longitude 45° at CR 2069. By CR 2079 it is centered at 90°. This is a slow drift relative to the Carrington rotation rate: 45° in 10 rotations, or $45/(25.38 \times 10) = 0.18$ deg d^{-1}.

Two blocks are selected from the longitude–time maps, each of length 1CR, and separated by 2CR. These are represented by the red and yellow boxes overlaid on Figure 3(a). These blocks are typically arrays of size 720 in longitude (0.5 bins) and 100 in time (0.01CR bins). Data gaps are treated as missing

data within the arrays. Cross-correlation of the density profiles can be performed as a function of the longitudinal lag. This is convenient computationally since the longitudinal density profiles can be wrapped around the $0^\circ/360^\circ$ boundary, enabling a complete circular shift from -180° to 180° for the cross-correlation. Trial and error shows that performing a global cross-correlation on extended blocks of the data gives clean and meaningful results. The blocks of data have rows along longitude θ and columns along the time (or Carrington rotation) t dimension. The first matrix is denoted x and the second y. The mean density of each row of x, or the mean density across longitude, is calculated as $\bar{x}_\theta$. The same operation is performed on y to give $\bar{y}_\theta$. Calculating the standard deviation along each row of x and y gives σ_x and σ_y, respectively. The longitudinal profiles are then normalized to a mean of zero and standard deviation of unity to give x_n:

$$x_n = \frac{x - \bar{x}_\theta}{\sigma_x}. \quad (1)$$

x_n therefore is a block of typically 100 longitudinal density profiles, with each individual profile averaged to zero and normalized to a standard deviation of unity. The same operation is performed on y to give y_n. If x_n and y_n have n_θ longitudinal bins indexed by i_θ, and n_t time bins indexed by i_t, the cross-correlation between x_n and y_n at lag l is calculated as

$$c_l = \frac{1}{N} \sum_{i_\theta=0}^{n_\theta-1} \sum_{i_t=0}^{n_t-1} x_l \, y_n, \quad (2)$$

where x_l is the x_n array shifted through lag l along the longitudinal dimension (a circular shift) and N is the number of valid data values. c_l is calculated for all longitude lags between -180° and 180°. For the example of the two arrays in Figure 3(a), c_l is plotted in Figure 3(b). There is a clear maximum peak in the correlation profile at lag 21°. That is, the best match between the red and yellow array is achieved when the red array is shifted to the right by 42 steps, or 21°. Since there is a 2CR time increment between the red and yellow arrays, the rotation rate is calculated as $21/(25.38 \times 2)$ deg d^{-1}, or 0.42 deg d^{-1} relative to the standard Carrington rotation rate. This is considerably higher than the value found by eye in the previous paragraph. This is because the drift of structure with time is not constant. Figure 3(a) shows that there is a rapid movement of the main high-density structure between the red block and the yellow. The example done by eye was an approximate estimate made over 10 Carrington rotations. The choice of time gap to study correlation is therefore important, and is dictated by the type of data. The tomography maps allow us to study the rotation rates at a resolution of a few CRs. Choosing a longer time gap and larger blocks of data for the correlation analysis gives a higher maximum peak in the correlation profile, but the peak is broader and less well defined. Too small a gap gives many low peaks in the correlation profile, and it becomes difficult to distinguish significant results from noise. The choice of block size of 1CR, separated by a gap of 2CR, is therefore a sensible compromise determined by trial and error, and which takes best advantage of the time resolution of the tomography maps. It is important to remember that a set of observations taken over half a Carrington rotation is needed to create a tomography density map, and any real changes in the corona at a timescale smaller than this will not be resolved, and will result in a more noisy and "smeared" tomography reconstruction.

As can be seen in Figure 3(b), there are often several peaks detected in the correlation profile. Most of these are not significant and do not give information on rotational rates. Our final results are formed by the argument that, in contrast to the true rotational rates, insignificant peaks are highly unlikely to form coherent groups of measurements over longitude and time. Initially, therefore, we set an arbitrarily low threshold to define a peak in the correlation profiles. This will keep the wanted rotational rates plus a lot of insignificant peaks caused by noise. A peak is defined as a maximum in a local neighborhood of $\pm 4.^\circ 5$ lag, with a correlation value of 0.1 or higher. For the example shown, this definition gives four peaks. Choosing which is significant from a single profile is impossible, but given a large number of consecutive measurements, it becomes possible to find coherent groups of peaks which give the final rotation rates. The correlation analysis is repeated throughout the whole observational period, with the time period of ~1CR shifted forward in small increments (0.1CR or so) through the whole set of tomography maps. At each step, all peaks are translated from a lag measurement into units of deg d^{-1}, and recorded. This results, for a given latitude, in hundreds of different rotation rates calculated over time. Since all peaks are recorded at each time step, the set of rotation rates can have a wide scatter and as such can be difficult to interpret. The final step of the analysis is to select only those rotation rates which are tightly grouped in high numbers, and to discard outlying points. The next steps describe the filter used to discard such outliers.

1. The set of points $X(R, t)$ are rotation rates R distributed in time t.
2. A two-dimensional histogram H_{ij} of measured rotation rates is calculated. The histogram records the number of points in $X(R, t)$ found within each discrete bin R_i, t_j. The i, j subscripts index the rotation rate and time bins, respectively. A bin size of 3CR and 0.2 deg d^{-1} is used here.
3. H_{ij} is smoothed to give S_{ij}. Here, we use a 5×5 boxcar average. It is a good practice to smooth the histogram to reduce the effect of imposing a discrete bin size.

To identify outliers, we need to find areas of H_{ij} which are less than a given threshold. However, it adds robustness and flexibility to define a threshold which adapts according to local conditions. Rather than use, for example, the mean value of H_{ij} (times a preset factor) to define a global threshold, it is possible to use a localized mean (times a preset factor). Here, we use a mean which is localized in time.

4. The mean of S_{ij} is calculated at each time bin j (over all rotation rates i at that time bin). This gives a function of time only, s_j, which is smoothed with a 5 wide boxcar average.
5. A global threshold factor f is used to control the tolerance of the filter. High values of f result in a stringent filter. A low value detects less outliers. To identify outliers, areas of S_{ij} which are less than $f.s_j$ are considered regions of low measurement density. Any member of X falling in such a region is discarded. f is set at 2.2 for this work.

This outlier filter removes much of the scatter from the measured rotation rates, leaving sensible values which show a good continuation over time. Its application is demonstrated in Figure 4, for equatorial rotation rates calculated from CR 2021 to 2080. Between CR 2060 and 2076, the rotation rates found using the correlation method are very clean, with little scatter. It can be seen from Figure 4 that the outlier filter leaves these measurements unchanged. Between CR 2021 and 2060, there

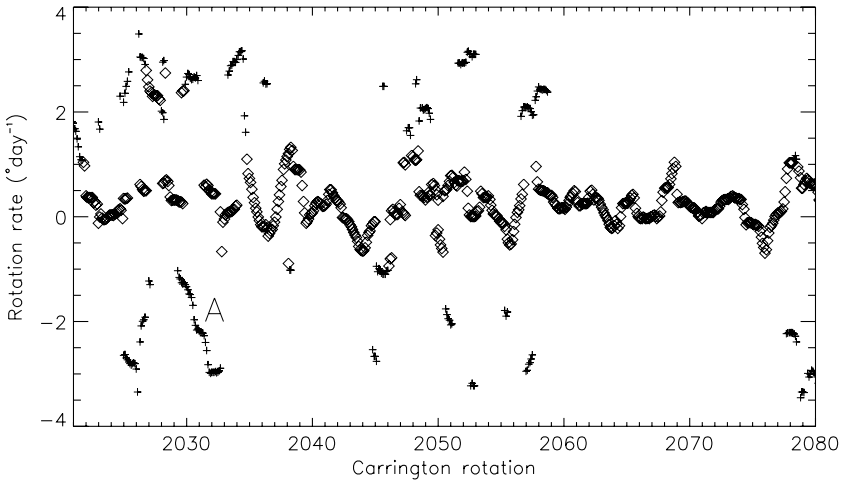

Figure 4. Rotation rates measured at the equator using the correlation analysis technique between CR 2021 and 2080. The complete set of peaks detected in the correlation profiles are shown here. Peaks which are identified as outliers, and ignored in further analysis, are shown as crosses. Peaks kept for further analysis are shown as diamonds. One group of outlying points, at CR 2030, rotation rate -2 deg d^{-1}, is labeled A.

is considerable scatter, but with the bulk of measurements approximately clustered within the ± 1 deg d^{-1} rotation rates. The filter keeps these measurements more or less without change, but removes the small groups of points isolated from the densest regions. One such group is labeled "A." It could be argued that such a group shows perhaps a rotational phenomenon which is real, since it seems as if the points describe a consistent linear acceleration over several Carrington rotations. Perhaps therefore a small coronal structure at this time is behaving differently to the bulk of structure at the equator, and is detected by both the tomography and the correlation technique. Because this study is concerned with the more long-term and dominant rotational rates, we discard such groups, and aim to study smaller-scale structural movement in a separate work.

In summary, many peaks are detected in the correlation profiles, and many of them will be caused by errors or possibly by short-lived movement of smaller-scale structure (which is not wanted for this study). The higher-level filter is applied to select only those peaks which belong to relatively tightly distributed groups which show a continuation in time. These tend to be the long-term and large-scale rotation rates since the values are dominated by the slow drift of the largest scale structure, which are also the longest lived and highest density structures. Over the timescales used for the correlation analysis, it is plausible that different structures at the same latitude can rotate at different rates. Structures can also drift in latitude, and the large-scale configuration of structure and the distribution of densities within that structure can change considerably, even rapidly. In addition, it seems as if structure can often move in sharp jumps rather than smoothly. This is seen in Figures 3(a) and 4, and is worthy of the further discussion given in Section 4.

3. RESULTS

Figure 5 shows several longitude–time maps of the coronal density at different latitudes between 1996 and 2010. Slow drifts in longitude of stable high-density streamers can easily be seen in these maps. The scale of the maps is such that only the longer-term persistent trends are apparent. Structures which describe vertical paths in these maps are rotating at the Carrington rotation rate of 14.18 deg d^{-1}, for example, the streamer at longitude $\sim 180^\circ$, latitude -60°, between CR 1990 and 2005. Structures which describe paths leaning toward the right (increasing longitude with time), such as most structure seen near the equator after $\sim$CR 1980, are rotating slightly faster than the Carrington rotation rate. Conversely, structures leaning to the left, such as that seen at latitude -60° at solar maximum, are rotating slower than the Carrington rotation rate. It is immediately apparent that the large-scale rotation of streamers varies with time over the solar activity cycle as well as with latitude.

Figure 6 shows the results of applying the long-term correlation analysis. Long-term rotation rates are generally close to the Carrington rotation rate, but show considerable and often surprising variation. The following sections summarize the rotational information contained in this figure, and are arranged by time periods: (Section 3.1) solar minimum and the fast rise to solar maximum (1997 to mid-1998, or the loss of *SOHO*), (Section 3.2) solar maximum (mid-1998, or the restoration of *SOHO* to the end of 2002, the end of the peak of solar maximum), and (Section 3.3) the slow return from maximum to minimum (the end of 2002–2010).

3.1. Solar Minimum and the Rise to Solar Maximum (CR 1915–1940)

It is difficult to study rotation during solar minimum since there are more frequent data gaps and non-standard observations during the initial few months of the *SOHO* mission. A separate study analyses the sporadic density maps for 1996–1997 (Morgan 2011). By 1997, there are fewer data gaps and the series of tomography maps becomes frequent enough to allow a correlation analysis and a closer study of the longitude–time contour maps of Figure 5. The brief period at the beginning of 1997 shows a rotation rate roughly consistent with that found in Morgan (2011), of around a few tenths of a deg d^{-1} below the Carrington rate. However, by mid-1997 the rotation at the equator is dominated by a slower rate of ~ -0.7 deg d^{-1}, with a coherent cluster of measurements at a higher rate of ~ 0.8 deg d^{-1}. The results of the correlation analysis for solar minimum are summarized in the histograms of Figure 7. In the equatorial band of Figure 5, the main rotation rate of -1 deg d^{-1} can be discerned by eye, confirming the rates found by the correlation analysis. However, the structure is complicated and not entirely consistent throughout this almost 2 year period. The slow rotation trend is more obvious at latitude 20°, where there

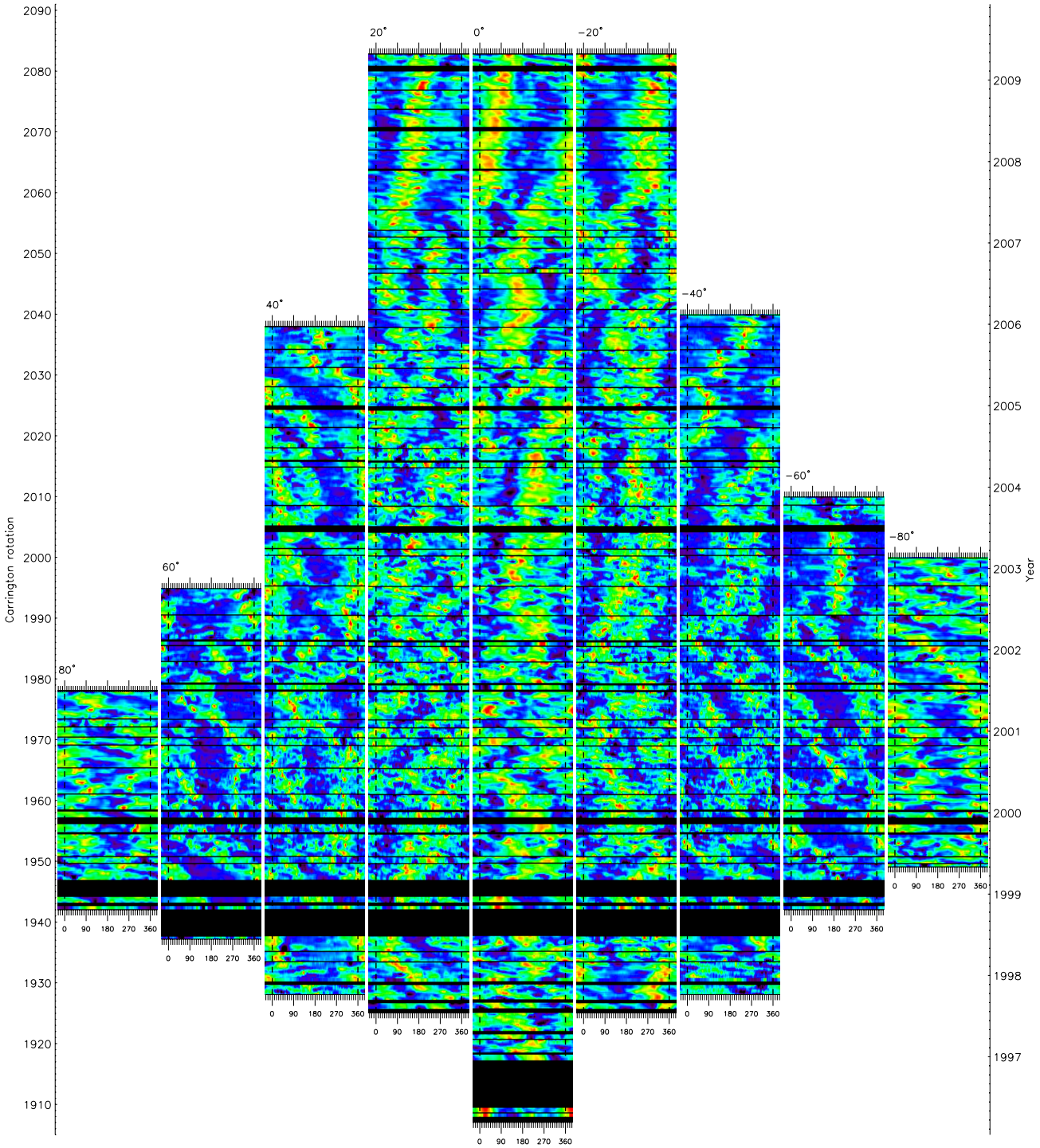

Figure 5. Longitude–time maps of the coronal density. The nine individual contour plots, arranged in columns, show the changing density at nine different latitudes, from latitude 80° to −80° in increments of 20° (latitude is labeled above each plot). The *x*-axis of each contour plot shows Carrington longitude. For clarity, the longitude is wrapped from −30° to 390°, and the two faint white dotted lines running vertically through each plot mark the positions of 0° and 360°. The left (right) *y*-axis shows Carrington rotation number from CR 1905 to 2090 (year from ∼1996 to 2010). The nine contour plots share the same time axis. At higher latitudes, the time range is approximately curtailed according to the times streamers exist at that latitude—that is why the figure is not symmetrical around the equator. Black areas which encompass all latitudes and longitudes are data gaps.

is a clear leaning of structure to the left throughout this period. This is confirmed by the correlation analysis, with most measured rates clustered within the −1 to −2 deg d^{-1} range. In the south, at −20° latitude, there is no evidence of slow rotation. To the contrary, rotation is dominated by rates ranging from 0 to 1 deg d^{-1} above the Carrington rate.

For a brief period of less than a year, before the long data gap caused by the loss of *SOHO* in 1998, streamers appear at latitudes 40° and −40°. The period is long enough to allow a correlation analysis, which shows slow rotation rates at both latitudes: approximately −0.5 deg d^{-1} in the north and more than −1 deg d^{-1} in the south. The result in the south is rather

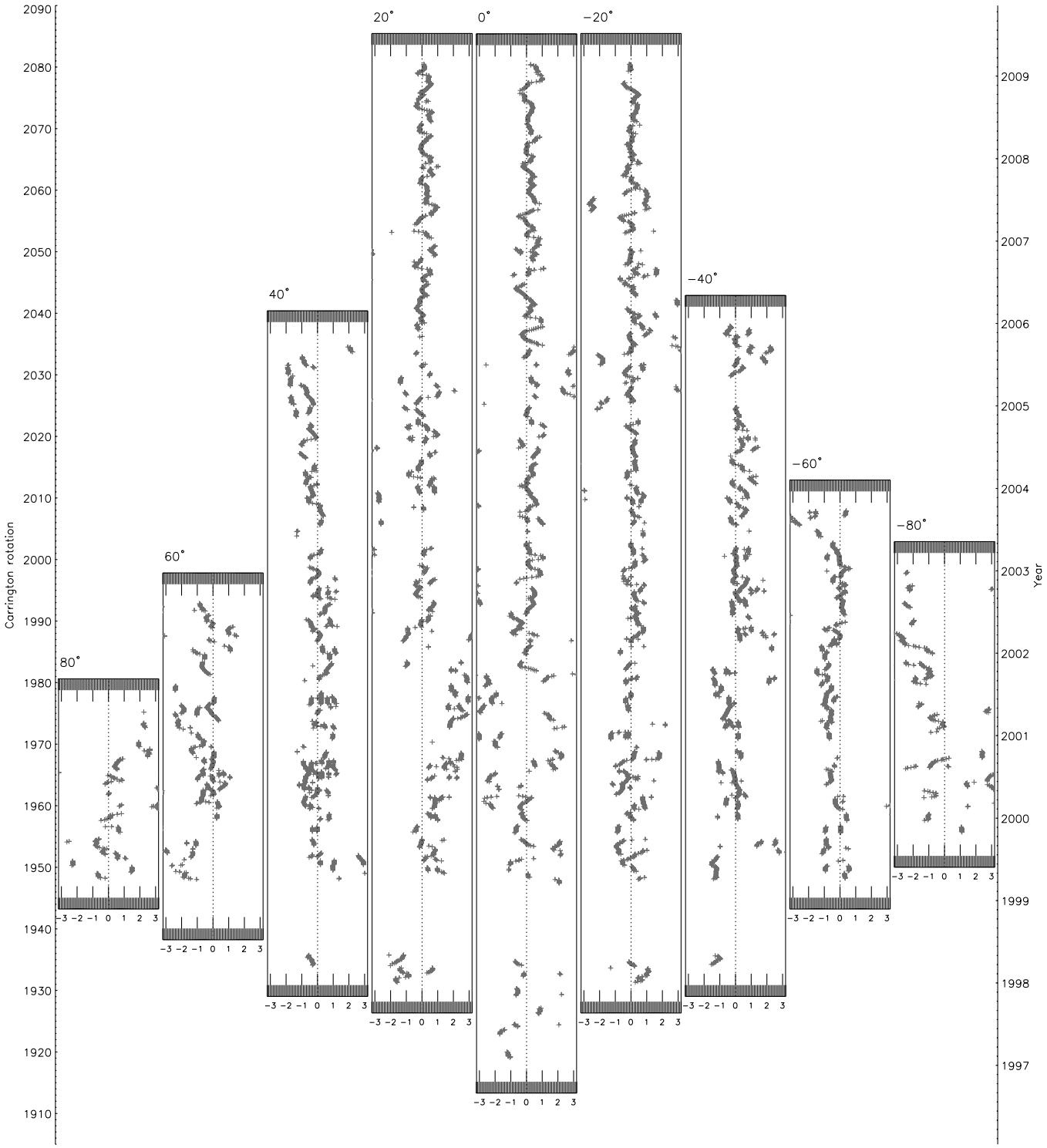

Figure 6. Rotation rates (given by crosses) as a function of time calculated using a cross-correlation method from the corresponding maps in Figure 5 (see the text). The nine individual plots, arranged in columns, show the changing rotation rate at nine different latitudes, from latitude 80° to −80° in increments of 20° (latitude is labeled above each plot). The *x*-axis of each contour plot shows the rotation rate in deg d^{-1} relative to the standard Carrington rotation rate of 14.2 deg d^{-1}. The faint dotted line running vertically through each plot marks the 0 deg d^{-1} or Carrington rotation rate. The left (right) *y*-axis shows Carrington rotation number from CR 1905 to 2080 (year from ∼1996 to 2009). The nine plots share the same time axis. At higher latitudes, the time range is approximately curtailed according to the times streamers exist at that latitude.

surprising since it is consistent with the slow rates found at all latitudes but contrary to the fast rates found at the neighboring latitude band of −20°, despite this neighboring latitude band lying between −40° and the other bands.

Figure 7 shows the sum of histograms at all latitudes considered in this section. There is a broad peak at 0.9 deg d^{-1}, containing contributions from latitude −20°. The majority of measurements are between −1.8 and −0.3 deg d^{-1}. There are

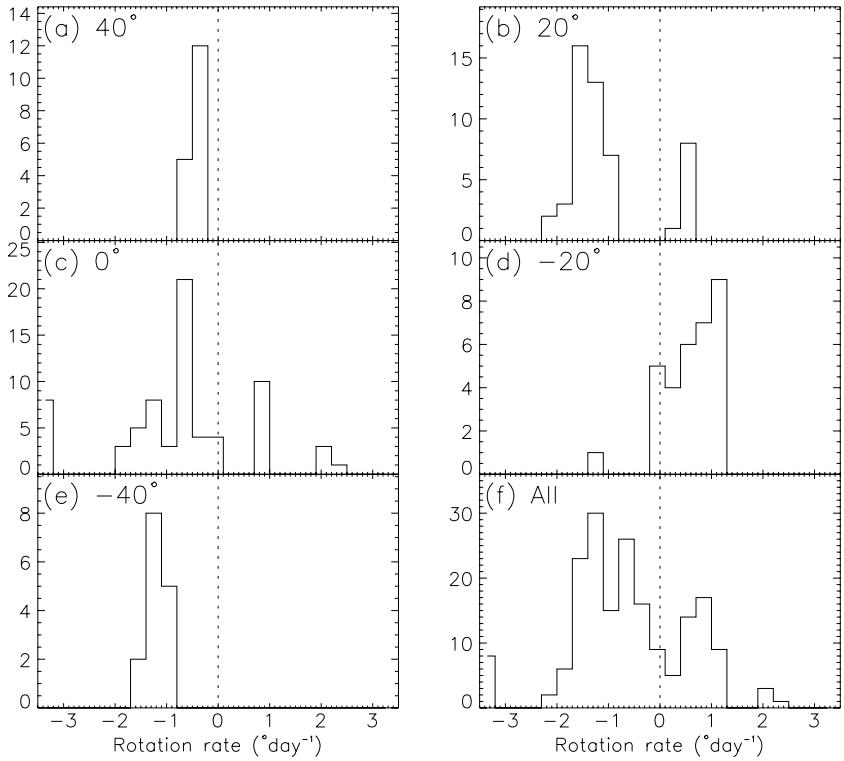

Figure 7. (a)–(f) Histograms of rotation rates as calculated using long-term correlation measurements at several latitudes for the period 1997–1998. The histograms are a summary of the information shown in Figure 6, extracting the appropriate time period. (f) Sum of the histograms at all latitudes (40° to −40°, or panels (a) to (e)). The *x*-axis of each plot shows the rotation rate in deg d^{-1} relative to the standard Carrington rotation rate of 14.2 deg d^{-1}. The dotted line running vertically through each plot marks the 0 deg d^{-1} or Carrington rotation rate. Measurements are summed over 0.3 deg d^{-1} bins.

not many measurements at the Carrington rate itself, and the highest peak is at −1.3 deg d^{-1}.

3.2. Solar Maximum (CR 1947–1995)

From CR 1947 to 1960, the equational rotation is dominated by rates within 1 deg d^{-1} of the Carrington rate, with some measurements at higher values of 2 deg d^{-1}. From CR 1960 to 1980, the structure is complicated and subject to rapid change. This is replicated in the correlation analysis, where values jump from slow to fast several times (from −3 to −2 deg d^{-1} slow, to 1 to 2 deg d^{-1} fast). After CR 1980, rates settle down again to values within ∼1 deg d^{-1} of the Carrington rate (and maintain this stability throughout the declining phase until the end of our study). This behavior during this period is seen in the histogram of Figure 8(e), where there are three separated bands of measured rotation rates, each approximately centered at −2.2, 0, and 1 deg d^{-1}.

The behavior at the equator is not replicated at nearby latitudes. At −20° latitude, rotation rates are distributed between −1 and 1 deg d^{-1} throughout solar maximum. Rates vary most between CR 1937 and 1970. After CR 1970, the rates are more narrowly restricted around the Carrington rate. Latitude 20° shows surprising behavior and is distinct from all other latitude bands—even neighboring bands. At CR 1947, rates are distributed somewhat higher than the Carrington rate. For the next 3 years, until CR 1980, there is a steady acceleration of rotation rates up to 3 deg d^{-1} above the Carrington rate. Following this acceleration, there is an abrupt return to rates close to the Carrington rate.

Rotation at latitude 40° is dominated by rates at, or slightly faster, than the Carrington rate. The most likely rate is the Carrington rate itself, as shown in the histogram of Figure 8(c), where there is a peak between 0.0 and 0.15 deg d^{-1}. Most values fall between 0 and 1 deg d^{-1}. For a few months surrounding CR 1963, rates are clustered at around −0.5 deg d^{-1}. At 60° latitude, rates are slower. Over the solar maximum period, the most likely rotation rate is the Carrington rate, but there are long periods spent at slow rates. From CR 1947 to 1954, rates are consistently between −1 and −3 deg d^{-1}. There follows a period of less than a year where structure is either rotating at the Carrington rate, or slightly slower. At CR 1970, rates are again slow, at around −2 deg d^{-1}, before returning to values between −1 and 0 deg d^{-1} at CR 1976. A brief period at fast rotation (1 deg d^{-1}) is measured at CR 1988. This coincides with a region in the contour map of Figure 5 which is difficult to interpret.

The contour map at latitude 80° is messy. Measured rotation rates are rather scattered and incoherent and do not conform to the expectation of slower rates which we would expect to find, especially when we consider the slow rates which are found for the neighboring latitude at 60° and the corresponding south pole latitude of −80°. The measured rates are clustered around 0 deg d^{-1}, with isolated clusters of measurements at higher rates (2–3 deg d^{-1}) and slow rates (−2.5 deg d^{-1}).

At latitude −40°, there is a sharp peak in the measured rotation rates, at just above the Carrington rate. Despite this, rotation is slow (below −1 deg d^{-1}) at CR 1947, and most of the measurements are in fact distributed at slow rates between −1.5 and 0 deg d^{-1} during the solar maximum period. At latitude −60°, the vast majority of measurements are below the Carrington rate, with high peaks in the histogram at −1 and −0.6 deg d^{-1}. The behavior of the rotation rates toward the end of the solar maximum period is interesting, as can be seen in Figure 6. Rates are consistently slow from CR 1970, at around

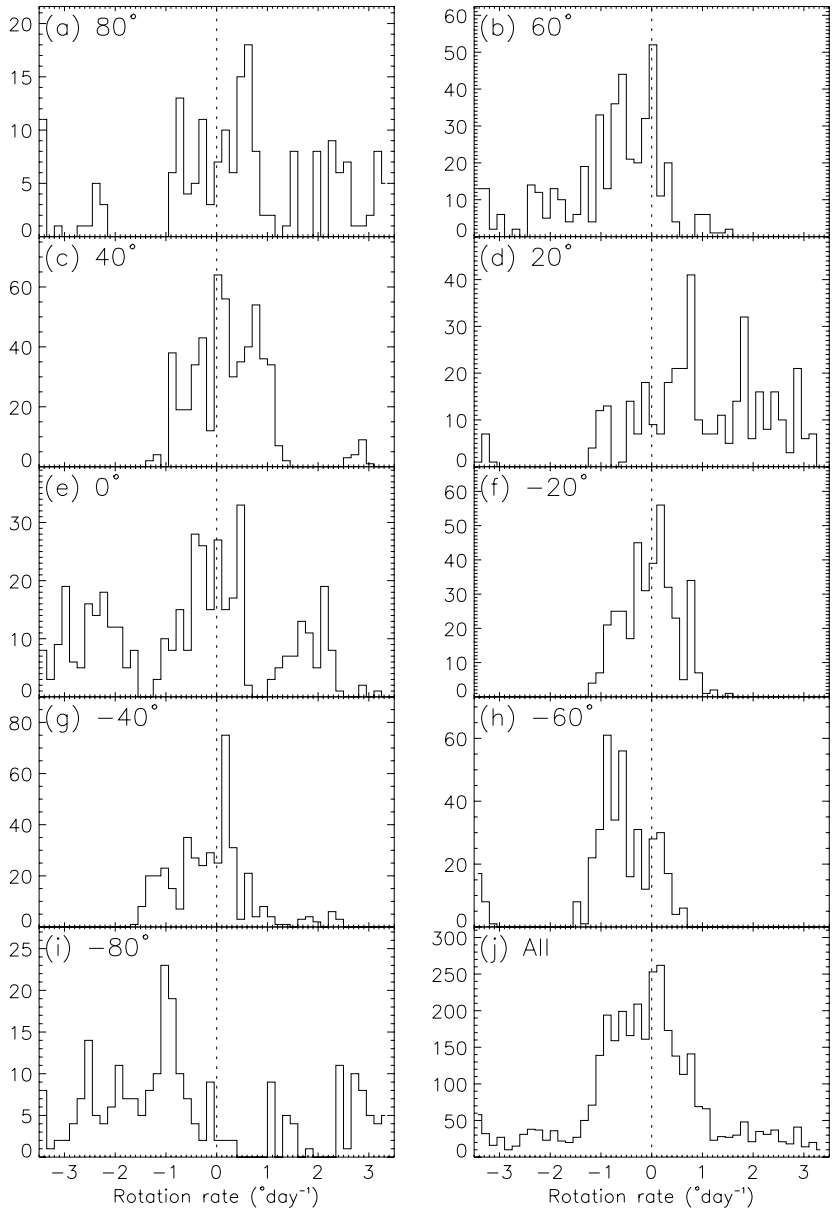

Figure 8. (a)–(i) Histograms of rotation rates as calculated using long-term correlation measurements at several latitudes for the period of a few years surrounding solar maximum. (j) Sum of the histograms at all latitudes (80° to −80°, or panels (a) to (i)). Measurements are summed over 0.15 deg d^{-1} bins.

−1 deg d^{-1}, and remain so for over a year. There is then a rapid but smooth change over a period of around half a year to rates around the Carrington rates, at which the rotation remains stable for around a year (or approximately until streamers disappear from this latitude).

Structure at latitude −80° is rotating somewhat more coherently than that seen at similar latitudes in the north. Between CR 1958 and 1970, rotation can be very slow, often between −3 and −2 deg d^{-1}, with a wide scatter. There are isolated measurements at high rotation rates of 1–3 deg d^{-1}, seemingly at odds with the dominant slow rates. This may be due to the unsuitability of the correlation analysis for measuring sporadic and rapid changes. Around CR 1970, measurements are clustered neatly around −0.5 deg d^{-1}. Six months later they decrease to below −1 deg d^{-1} and slower, ending the period between −3 and −2 deg d^{-1}. The histogram of Figure 8(i) shows that most measured rates are between −3 and 0 deg d^{-1}, with three separated peaks at −2.7, −1.8, and −1 deg d^{-1} (the latter being the most prominent).

The histogram of Figure 8(j) shows the overall histogram for this period across all latitudes. There is a substantial distinct peak at rotation rates between 0 and 0.3 deg d^{-1}. The bulk of measurements are between −1.15 and 0.75 deg d^{-1}, and ignoring the peak at 0–0.3 deg d^{-1}, this distribution is skewed toward slower rates.

3.3. Declining Phase (CR 1995–2090)

This long period of slow decrease in solar activity, and in the slow decrease in latitude of streamers from the poles to mid-latitudes and regions close to the equator, is accompanied by the period of most coherent and steady rotation. Figure 9(c) shows rotation rates for the equator for this period. The majority of rates are between −0.15 and 0.6 deg d^{-1}, with peaks at 0 and 0.45 deg d^{-1}. Rates are in general slightly slower for latitudes

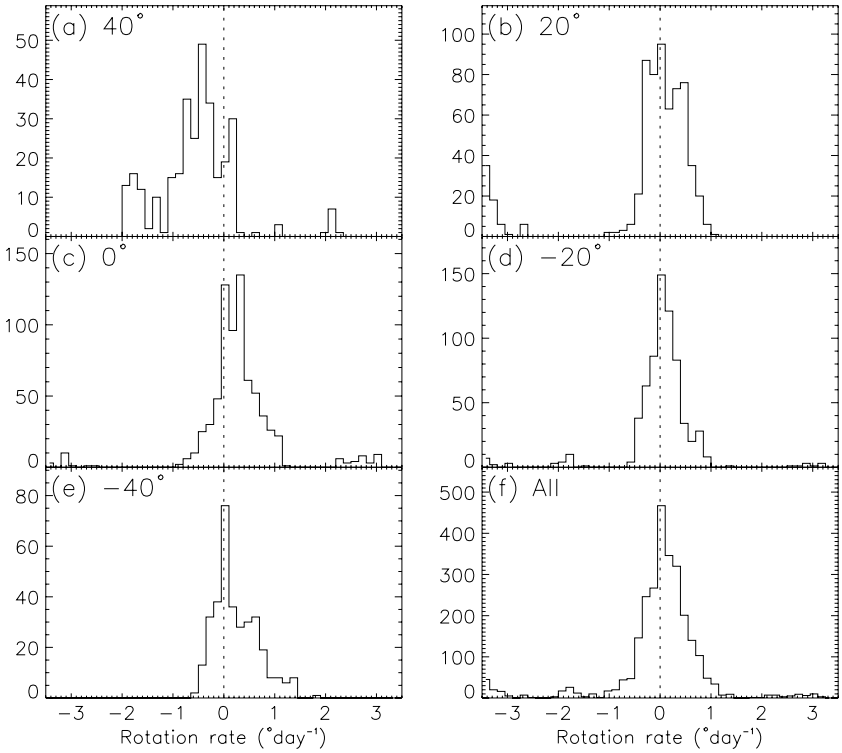

Figure 9. (a)–(e) Histograms of rotation rates as calculated using long-term correlation measurements at several latitudes for the declining period after solar maximum. (f) Sum of the histograms at all latitudes (40° to −40°, or panels (a) to (e)). Measurements are summed over 0.15 deg d^{-1} bins.

20° and −20°. At latitude −20°, rates are narrowly distributed around an average of 0.05 deg d^{-1} (whereas the average rate for the equator is 0.24 deg d^{-1}). At latitude 20°, there is a wider distribution, peaking at 0 deg d^{-1}, with an average of 0.1 deg d^{-1}.

At latitude −40°, the majority of measurements are at the Carrington rate. The distribution is relatively narrow, and skewed toward rates faster than the Carrington rate. This is contrary to the results for latitude 40°. Rates here begin at the Carrington rate at CR 1995, then seem to decelerate toward values of around −2 to −1 deg d^{-1}. There seems also to be evidence of two rates in coexistence since the correlation analysis detects two distinct bands of rates separated by around 1 deg d^{-1}, both decelerating smoothly to −2 and −1 deg d^{-1}.

4. DISCUSSION

Figure 10 shows rotation rates as a function of latitude. Figure 10(a) shows values averaged across all time from the rates displayed in Figure 6 using a weighted mean determined by the height of the individual correlation peaks (so a high correlation peak gives more contribution to the final mean). The error bars give a weighted variance of the rotation rates, so give a measure of the variance over time rather than any error in measurement. The rotation rates near the equator are, on average, just slightly higher than the Carrington rate. Rotation rates are more or less constant up to latitudes of ∼40° from the equator. Rates are then slower up to latitudes ∼60° or so. As discussed above, it is difficult to trust the rotation rates found at 80° north. The latitudinal profile is very similar to the results typically given by flux modulation studies. Averaged over time, the coronal rotation is far more rigid than the photosphere. However, this study reveals that the corona does experience considerable differential rotation, albeit a differential rotation which is localized in time and latitude and is hidden when values are averaged over time.

Plotted on Figure 10(a) is a curve found by Fisher & Sime (1984) to fit the latitudinal profile of rotation rates found by flux modulation of several years (1965–1983) of Mauna Loa K-coronameter data. Considering that the curve was found for different solar cycle, height, instrument, and analysis method, the agreement is excellent. The rotation rate measurements of Fisher & Sime (1984) show considerable variation over the 17 years, on the same order as the variation found in this study.

Figures 10(b)–(d) show the latitudinal dependence of rotation rates averaged over different time periods. There are clear trends here, with solar minimum showing slowest rotation. Fastest rotation is at mid-latitudes at solar maximum. The cleanest evidence of a long-term north–south asymmetry is during the declining phase, and the results with least variance are also seen during this time. The fast rate measured at −20° latitude during solar minimum is seen to affect a broad latitude band extending from −10° to −30°, but with the peak rotation rate at −20°.

Overplotted on Figures 10(b) and (c) are latitudinal profiles of rotation rates found by Giordano & Mancuso (2008) and Mancuso & Giordano (2011) for solar minimum and maximum, respectively. The agreement for solar minimum is poor. The measurements of Giordano & Mancuso (2008) were made using O VI 1032 Å emission at a height of 2 $R_\odot$, and this may partly explain the disagreement. The O VI measurements may well be dominated by the rotation of one bright structure rather than the general distribution of streamers, leading to faster rotation rates and underestimation of variation. In contrast, the agreement during solar maximum is good, and the estimate of variation is better but still too small. Tracer studies of rotation in the photosphere, chromosphere, and low corona often give results with large variation (see, for example, Figure 1 of Wöhl et al. 2010 for coronal bright points in EUV observations). A well

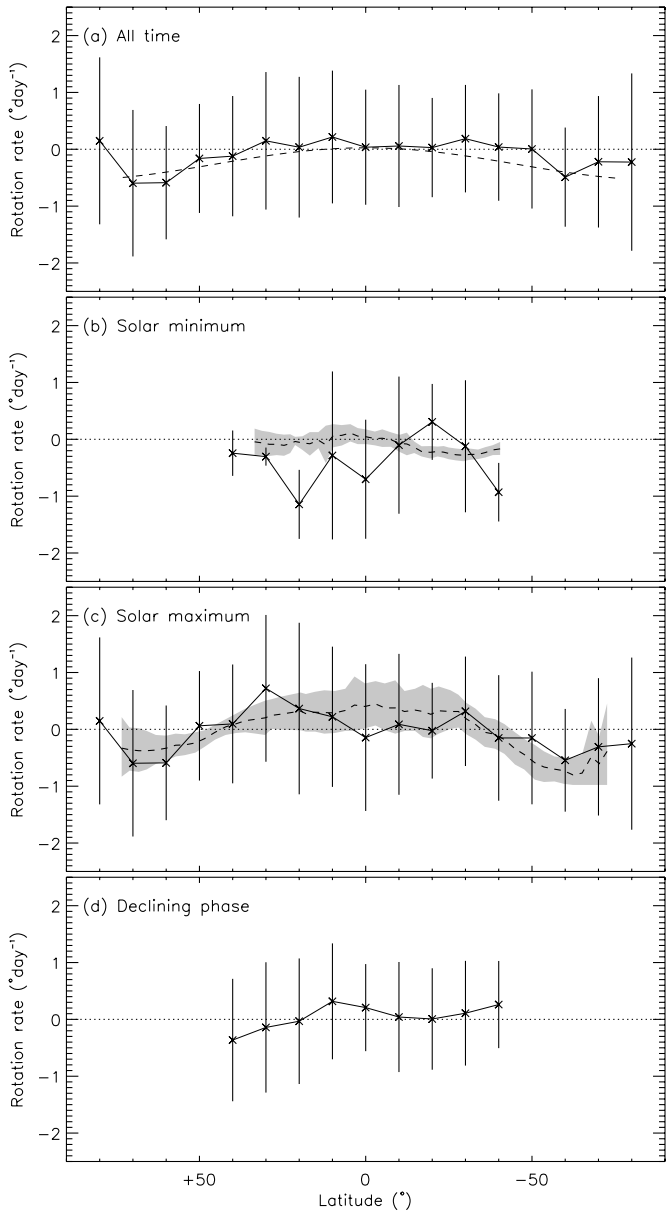

Figure 10. Solid line crossed with error bars shows latitudinal dependence of rotation rates averaged across (a) all time, (b) solar minimum, (c) solar maximum, and (d) declining phase. Each point is a weighted mean of all measured correlation peaks at that latitude. The weights are given by the value of the correlation peak (therefore high correlation gives a greater weight toward the final mean). The error bars show a similarly weighted standard deviation of rotation rates during that time period. Rotation rates are relative to the Carrington rate (0 deg d^{-1}), shown as a dotted line. The dashed line in (a) shows a fit to rotation rates found by Fisher & Sime (1984) for years 1965–1983 using flux modulation of Mauna Loa K-coronameter data at heights close to 1.5 $R_{\odot}$. The dashed lines and gray shaded regions in (b) and (c) show the mean and standard deviation of latitudinal rotation rates at heights close to 2 $R_{\odot}$ found by Giordano & Mancuso (2008) for solar minimum (b) and Mancuso & Giordano (2011) for solar maximum (c).

behaved differential rotation curve is then found as an average of many points over time. There is no reason why the corona should behave differently, and this study finds that coronal streamers have large variations in rotation rates, but an average differential rotation curve which agrees with flux modulation studies (see Section 1). As can be seen from Figure 6, where rotation rates are shown as a function of latitude and time, the apparent simple rigid rotation of the corona shown in Figure 10 is not always the correct picture. Also apparent in this study is that the rotation rates seem to vary on small timescales (that is, on the order of a few months).

It is difficult to determine the rotation of an object which changes shape. The clearest set of measurements given by this study is for regions between the equator and mid-latitudes for times during the descending phase after solar maximum. This is a time when the corona is structurally stable on large scales. Streamers stay at the same latitudes for long times, and there are only slow drifts in longitude. During the rise to solar maximum, and especially during solar maximum itself, there are times when assigning a rotation rate to the corona is difficult (and perhaps invalid) because the dominant movement in the corona is one of rapid reconfiguration—particularly for certain latitude bands during the height of solar maximum. The poles and the equator in particular show little coherent structure over long time periods to allow a study of rotation using current observations and analysis techniques. This immediately raises questions about the validity of determining coronal rotation using flux modulation at these times. Lewis & Simnett (2001) state that during their solar maximum measurements, only one or two repeat peaks typically appear in their autocorrelation functions. Any rapid reconfiguration will make the tomography reconstructions more noisy and prone to error, and will make any type of rotational study using current observation and methods void—whether it be by flux modulation or tomography.

An important point therefore is the timescale at which rotation, or coronal evolution in general, is measured. The tomography takes half a solar rotation to create one density map, so any movement more rapid than this will appear as noise, or smeared (smoothed) in a time series of tomography maps. At the other extreme, any comparison of structure between time steps of more than a few Carrington rotations is not so useful to reveal rotation since it is likely that structural reconfiguration has occurred, obscuring any apparent rotation rates. The approach taken in this study of using a time step of 2CR to compare structures is therefore a choice which gives reasonable results most of the time, but is still not useful at some latitudes during some periods. The nature of the coronal evolution during these periods will only be revealed by advances in observation, probably by multiple spacecraft giving a more instantaneous picture of the 3D coronal structure than that given by current tomography. The *STEREO* mission (Kaiser 2005) offers an improvement in this regard. The *STEREO*/SECCHI coronagraphs have been used for tomography (see Vásquez et al. 2011, and references within), although the two-spacecraft viewpoint configuration has yet to be fully exploited.

This study shows that it is highly probable for a range of rotation rates to be present over short time periods. Occasionally the results suggest that different rotation rates are present simultaneously. This is feasible if there are several streamers distributed in longitude—even just two streamers possessing different rotation rates. This lends some support to the study of rotation within a PFSS model made by Hoeksema & Scherrer (1987), where two main periodicities were found.

The false expectations of a rigidly rotating and smoothly evolving corona may be based on several premises: (1) extensive studies of photospheric or chromospheric/low-coronal features where well behaved rotation is measured in great detail over many decades, and the desire to find a similar behavior in the corona. The corona is different, however, in that plasma movements can be dictated by large-scale reconfigurations of the coronal magnetic field—and such reconfigurations may be relatively rapid, certainly on the scale of a few Carrington

rotations. (2) The results of Potential Field models do not change rapidly, particularly during solar minimum. However, Morgan (2011) shows that despite the stability of a PFSS model between 1996 and 1997, the density pattern revealed by tomography within the magnetic field configuration does change. (3) Flux modulation analyses which give well behaved, smooth results, but in fact are time-averaged values of a spatially smoothed measurement (i.e., LOS integration), hide much of the more interesting small-scale movement.

As the photosphere differentially rotates, evolves over the solar cycle, and, on shorter timescales, as photospheric magnetic features appear and dissipate, the corona must keep in step. Magnetic tension may build up and release, and rapid reconfigurations may be superimposed on a more smooth underlying rotation. An additional complexity is the link between the corona and the photosphere. Oscillating between solar minimum and maximum, the large-scale dipole component of the coronal field becomes dominant then weak, and streamers at a given latitude at a height of 4 $R_\odot$ are linked to very different latitudes at the photosphere. This may explain very abrupt changes in rotation rates, and abrupt changes in the spatial distribution of streamers at a given latitude. A good example is near CR 1990 at latitude -60° in the south. There is an abrupt change from slow rotation rates to rates near the Carrington rate, accompanied by a rapid structural reconfiguration (see Figures 5 and 6). There is no obvious sign of a reconfiguration from visual inspection of coronal images: the rapid change in structure is apparent only using tomography.

Perhaps the most surprising result of this study is how neighboring latitudes are at times rotating at very different rates, for long periods of time. One of the most striking examples is at latitude -20° during solar minimum (see Figure 5). This rotational behavior is rather difficult to interpret, and places an interesting challenge on large-scale models of the extended corona. Is interchange reconnection behaving differently at some latitude bands compared to others? Certainly the rate of interchange reconnection must vary depending on the inclination of the boundary between closed and open field regions (i.e., inclined north–south, we would expect higher rates of interchange reconnection; see Lionello et al. 2005), and this may result in different rotation rates at extended coronal heights. Streamers at this latitude may be more strongly rooted in different latitudinal regions, or structural features, of the photosphere which are rotating faster than the general photospheric–coronal connections. The coronal structure in the south is a pseudostreamer (i.e., a streamer not connected with the main neutral sheet—see Wang et al. 2007 or Section 7 of Morgan & Habbal 2010b), and is perhaps evolving differently from the streamers embedded in the neutral sheet at other latitudes.

At solar minimum, and during the descending phase, the large stable streamers at 4 $R_\odot$ are rooted at the Sun above the equator and up to mid-latitudes. The poleward footpoints of these large helmet streamers are associated with longitudinally aligned filaments, or the photospheric magnetic neutral lines which underlie the filaments (Morgan & Habbal 2007). During solar minimum, the single streamer belt at heights above $\sim 3\ R_\odot$is also approximately aligned longitudinally (i.e., at a constant latitude). The same configuration is found during the descending phase, although there are two separate streamer belts in the north and south (see Morgan & Habbal 2010b). Such a parallel configuration of helmet streamers (where the longitudinally extended sheets of high density in the corona are aligned with the longitudinally extended streamer footpoints at the chromosphere/transition region) is stable and leads to minimal tension. As the photosphere differentially rotates, with latitude and time, and the footpoints of coronal streamers are subject to interchange reconnection and tension, the alignment of the streamers is such that they can adjust in a well behaved manner. At solar maximum, coronal density sheets are not longitudinally extended (i.e., they can span a range of latitudes), and they are less likely to lie parallel to their sources at the Sun. In addition, their sources at the Sun extend to higher latitudes. The magnetic field configuration between the Sun and the radial corona ($\sim 3\ R_\odot$) is complicated and more twisted. Differential rotation at the Sun will therefore create greater reconnection rates and force more rapid changes in the extended corona.

This study limits the analysis to high-density streamers. No other structures are detected by the tomography—only high-density streamers and regions void of streamers (which are dominated by noise). No polar plumes, for example, are detected at high latitudes during solar minimum. The correlation analysis could well be dominated at times by the radial extension of coronal holes, since the distribution of high electron density streamers is, by definition, dictated by the distribution of low electron density coronal holes. There is currently no simple way of measuring the rotation of plumes (and therefore the polar magnetic field during solar minimum) at appreciable heights in the corona. This raises questions on the ability of previous flux modulation studies in determining rotation rates for very high latitudes in the corona at times during solar minimum.

4.1. Technical Implications for Coronal Tomography

Tomography of the solar corona depends on the rotation rate. For the tomography maps which form this study, the Carrington rotation rate was used. Thus, each observation forms a view of the corona at a certain observing angle which changes with time. The angle used to backproject the observations through a computational volume to create the 3D reconstruction of coronal density is based of course on the chosen rotation rate. Using an incorrect rotation rate will undoubtedly cause error in the reconstruction. This error may well contribute to a persistent problem in SRT—small regions of the reconstruction which contain zero density (or negative density in an unconstrained reconstruction—see Frazin 2000, for example). This study shows that the rotation rate is sometimes far from the Carrington rate. An improvement to coronal tomography would be to use the rotation rates found (using the tomography and the initial Carrington rotation rate) to recompute the coronal density at a more appropriate rotation rate for any given latitude. This one-step iteration should be sufficient to give more accurate reconstructions although no major qualitative differences are expected compared to current results.

5. CONCLUSIONS

A large set of density structure maps calculated using tomography from the observations of the LASCO C2 coronagraph has given a fresh insight into the evolution of the coronal structure over a solar activity cycle (1996–2010). The maps have allowed rotation rates to be measured, without the LOS uncertainty inherent to flux modulation studies, at all latitudes and times where streamers exist. Averaging rotation rates over the whole solar cycle gives rotation slightly faster than the Carrington rate at the equator up to mid-latitudes of 40°–50°, and slightly lower rates at higher latitudes (~ -0.5 deg d^{-1}). These results are similar to those of previous flux modulation studies, with rotation

more rigid than the photosphere, but with a small amount of differential rotation.

The averaging of rates found over the cycle hides many of the interesting features found at shorter timescales, and may actually be misleading. The rotation of the corona is not latitudinally rigid. Indeed, at many times, large variation of rotation rates is measured. Rates are dominated by the Carrington rate, but at many times over the solar cycle, distinct peaks in the histograms of rotation rates are measured between -3 and 3 deg d^{-1}. Rotation rates can vary considerably between latitudes, even simultaneously between neighboring latitudes. This raises questions about the interpretation of previous flux modulation studies, where signals over time periods of typically a year are used to calculate rotation, and averaging over even longer time periods is often applied to find a latitudinal dependence. Such averaging obscures interesting and potentially insightful features of the coronal rotation.

Rotation rates can remain relatively stable or change smoothly over long periods of times, or can change rather abruptly. Solar minimum is dominated by slow rotation rates at all latitude bands except for -30° to -10°, where faster rotation is seen, peaking at -20° latitude. This behavior is interesting since this band of faster rotation is sandwiched between two bands of slow rotation. At the equator and poles at solar maximum, the movement is dominated at times by rapid structural reconfiguration, and not a coherent rotation. During these times, it is not so useful to discuss the structure of the corona in terms of a rotation. On average, fastest rotation is seen at $\pm 30^\circ$ latitudes during solar maximum. The most well behaved rotation is seen during the long declining phase, with rates close to the Carrington rates and, when averaged over the period, a slow increase in rotation is seen from north to south.

The interpretation of such behavior must be in terms of a complex interplay between photospheric/sub-photospheric differential rotation, the latitude and structures where coronal streamers are rooted at the photosphere, rates of reconnection and the relative alignment of closed and open field in the lowest corona, the relative alignment of coronal density sheets and photospheric footpoints of streamers, and the corona's large-scale response to photospheric reconfigurations. Such an interplay will hopefully be observed as emergent behavior within advanced global MHD models in the future. In summary, these results raise new questions regarding the link between the Sun and the corona, and provide fresh challenges to interpretations of the coronal structural evolution and the development of large-scale coronal models. In particular, does interchange reconnection provide an explanation of the considerable latitudinal differences in rotation rates, and what mechanism can explain abrupt changes in rotation rates?

I am very grateful for the comments by an anonymous referee which have greatly improved this work. This work is supported by an NSF SHINE Award AGS-0962716, and NASA grants NNX07AH90G and NNX08AJ07G to the Institute for Astronomy. The *SOHO*/LASCO data used here are produced by a consortium of the Naval Research Laboratory (USA), Max-Planck-Institut fuer Aeronomie (Germany), Laboratoire d'Astronomie (France), and the University of Birmingham (UK). *SOHO* is a project of international cooperation between ESA and NASA.

REFERENCES

Adams, W. M., & Tang, F. 1977, Sol. Phys., 55, 499
Altrock, R. C. 2003, Sol. Phys., 213, 23
Antonucci, E., & Dodero, M. A. 1977, Sol. Phys., 53, 179
Antonucci, E., & Svalgaard, L. 1974, Sol. Phys., 34, 3
Badalyan, O. G. 2010, New Astron., 15, 135
Badalyan, O. G., Obridko, V. N., & Sýkora, J. 2006, Astron. Rep., 50, 312
Beck, J. G. 2000, Sol. Phys., 191, 47
Brajša, R., Ruždjak, V., Vršnak, B., et al. 2000, Sol. Phys., 196, 279
Brajsa, R., Vrsnak, B., Ruzdjak, V., Schroll, A., & Pohjolainen, S. 1991, Sol. Phys., 133, 195
Brueckner, G. E., Howard, R. A., Koomen, M. J., et al. 1995, Sol. Phys., 162, 357
Chandra, S., Vats, H. O., & Iyer, K. N. 2010, MNRAS, 407, 1108
Fisher, R., & Sime, D. G. 1984, ApJ, 287, 959
Fisk, L. A. 2001, J. Geophys. Res., 106, 15849
Frazin, R. A. 2000, ApJ, 530, 1026
Gigolashvili, M. S., Japaridze, D. R., Mdzinarishvili, T. G., Chargeishvili, B. B., & Kukhianidze, V. J. 2007, Adv. Space Res., 40, 976
Giordano, S., & Mancuso, S. 2008, ApJ, 688, 656
Hansen, R. T., Hansen, S. F., & Loomis, H. G. 1969, Sol. Phys., 10, 135
Hara, H. 2009, ApJ, 697, 980
Hoeksema, J. T., & Scherrer, P. H. 1987, ApJ, 318, 428
Howard, R. 1984, ARA&A, 22, 131
Insley, J. E., Moore, V., & Harrison, R. A. 1995, Sol. Phys., 160, 1
Jordan, C. 1969, MNRAS, 142, 501
Kaiser, M. L. 2005, Adv. Space Res., 36, 1483
Karachik, N., Pevtsov, A. A., & Sattarov, I. 2006, ApJ, 642, 562
Kariyappa, R. 2008, A&A, 488, 297
Lewis, D. J., & Simnett, G. M. 2001, Sol. Phys., 200, 75
Lewis, D. J., Simnett, G. M., Brueckner, G. E., et al. 1999, Sol. Phys., 184, 297
Lionello, R., Riley, P., Linker, J. A., & Mikić, Z. 2005, ApJ, 625, 463
Mackay, D. H., Priest, E. R., & Lockwood, M. 2002, Sol. Phys., 207, 291
Makarov, V. I., & Tlatov, A. G. 1997, Astron. Rep., 41, 543
Mancuso, S., & Giordano, S. 2011, ApJ, 729, 79
Morgan, H. 2011, ApJ, 738, 190
Morgan, H., & Habbal, S. 2010a, ApJ, 711, 631
Morgan, H., & Habbal, S. R. 2007, A&A, 464, 357
Morgan, H., & Habbal, S. R. 2010b, ApJ, 710, 1
Morgan, H., Habbal, S. R., & Lugaz, N. 2009, ApJ, 690, 1119
Morgan, H., Habbal, S. R., & Woo, R. 2006, Sol. Phys., 236, 263
Mouradian, Z., Bocchia, R., & Botton, C. 2002, A&A, 394, 1103
Nash, A. G., Sheeley, N. R., Jr., & Wang, Y. 1988, Sol. Phys., 117, 359
Navarro-Peralta, P., & Sanchez-Ibarra, A. 1994, Sol. Phys., 153, 169
Obridko, V. N., & Shelting, B. D. 1989, Sol. Phys., 124, 73
Parker, G. D., Hansen, R. T., & Hansen, S. F. 1982, Sol. Phys., 80, 185
Roša, D., Brajša, R., Vršnak, B., & Wöhl, H. 1995, Sol. Phys., 159, 393
Schroeter, E. H. 1985, Sol. Phys., 100, 141
Shelke, R. N., & Pande, M. C. 1985, Sol. Phys., 95, 193
Sime, D. G., Fisher, R. R., & Altrock, R. C. 1989, ApJ, 336, 454
Sykora, J. 1994, Adv. Space Res., 14, 73
Ternullo, M. 1987, Sol. Phys., 112, 143
Thompson, M. J., Christensen-Dalsgaard, J., Miesch, M. S., & Toomre, J. 2003, ARA&A, 41, 599
Timothy, A. F., Krieger, A. S., & Vaiana, G. S. 1975, Sol. Phys., 42, 135
Tlatov, A. G. 2006, Astron. Rep., 50, 325
Vásquez, A. M., Huang, Z., Manchester, W. B., & Frazin, R. A. 2011, Sol. Phys., in press (DOI: 10.1007/s11207-010-9706-1)
Vats, H. O., & Chandra, S. 2011, MNRAS, L219
Wang, Y., & Sheeley, N. R., Jr. 2004, ApJ, 612, 1196
Wang, Y.-M., Sheeley, N. R., Jr., & Rich, N. B. 2007, ApJ, 658, 1340
Weber, M. A., Acton, L. W., Alexander, D., Kubo, S., & Hara, H. 1999, Sol. Phys., 189, 271
Wöhl, H., Brajša, R., Hanslmeier, A., & Gissot, S. F. 2010, A&A, 520, A29
Wolfson, R., Bhattacharjee, H., & Dlamini, B. 1996, ApJ, 463, 359
Zaatri, A., Wöhl, H., Roth, M., Corbard, T., & Brajša, R. 2009, A&A, 504, 589